ELSEVIER

Cement & Concrete Composites 25 (2003) 599–605

Cement & Concrete Composites

www.elsevier.com/locate/cemconcomp

An investigation of fracture initiation and resistance-curve behavior in concrete

J. Lou [a], K. Bhalerao [b], A.B.O. Soboyejo [b], W.O. Soboyejo [a,*]

[a] Department of Mechanical and Aerospace Engineering, Princeton Materials Institute, Princeton University, Princeton, NJ 08544, USA
[b] Department of Food, Agricultural and Biological Engineering and Department of Aerospace Engineering, The Ohio State University, Columbus, OH 43210, USA

Abstract

This paper examines the effects of mix strength on the fracture initiation and resistance-curve behavior of concrete. The fracture initiation toughness and the resistance-curve behavior are shown to increase with increasing mix strength. However, the extent of stable crack growth is shown to decrease with increasing mix strength. The measured resistance-curve behavior is associated with the beneficial effects of crack-tip shielding due to ligament bridging mechanisms. The observed small- and large-scale bridging phenomena are then modeled using fracture mechanics models. The studies show that the measured resistance-curve behavior is predicted largely by considering the beneficial effects of ligament bridging. Finally, the implications of the results are then discussed for the design of durable concrete structures.

Keywords: Concrete; Fracture initiation; Resistance-curve behavior

1. Introduction

Significant efforts have been made to understand the toughening components that contribute to the fracture toughness of concrete [1–4]. These studies have shown that stable crack growth in concrete is generally associated with the formation of bridging ligaments and anti-shielding/shielding microcracking zones, as shown schematically in Fig. 4. The shielding components due to crack bridging in concrete have also been modeled by a number of researchers [1–4]. However, the absence of experimental stress–displacement functions has prevented the widespread use of the models developed in prior work on the modeling of crack-tip shielding in concrete [1–4].

This paper presents a simple mechanics framework for the modeling of toughening due to ligament bridging in concrete. The framework which is an extension of existing small- and large-scale bridging concepts [5–22], is applied to the prediction of resistance-curve behavior and geometry-independent steady-state toughness values. The model is applied to the prediction of resistance-curve behavior and steady-state toughness in concrete mixes with strength levels of 30, 35 and 40 MPa. The measured resistance-curves are shown to be in close agreement with the predictions from small- and large-scale bridging models. The implications of the models are then discussed for the design of durable concrete structures.

2. Micromechanical modeling

The problem of small-scale bridging (small bridging zone compared to crack size) was modeled analytically by Budiansky et al. [5]. Assuming either rigid/perfectly plastic, or elastic perfectly plastic behavior, they obtained a number of solutions for the estimation of toughness due to crack bridging by ductile particles. Most of the expressions in Ref. [5] do not include a bridging length scale. However, one of the equations, which was obtained essentially from Tada et al. [6], did include a bridging length scale. This gives the toughening ratio due to crack bridging, λ_b, to be:

* Corresponding author.
E-mail address: soboyejo@princeton.edu (W.O. Soboyejo).

0958-9465/02/$ - see front matter
doi:10.1016/S0958-9465(02)00073-2

$$\lambda_b = \frac{K}{K_m} = 1 + \sqrt{\frac{2}{\pi}} \frac{f}{K_m} \int_0^L \frac{\alpha\sigma(x)}{\sqrt{x}}\,dx \quad (1)$$

where α is a constraint/triaxiality factor, $\sigma(x)$ represents the bridging traction across the ductile reinforcements, x is the distance from the crack face behind the crack-tip, and L is bridging length, which is equal to the distance from the crack-tip to the last unfractured reinforcement.

The above analysis applies largely to the problem of small-scale bridging. In the cases where the lengths of the bridging zones are comparable to the overall crack dimensions, large-scale bridging models are needed to estimate the shielding contributions from crack bridging. The early large-scale bridging models were first formulated by Odette et al. [7] and Zok and Hom [8]. Subsequent work by Cox and co-workers [9,10] also established self-consistent methods for the analysis of large-scale crack bridging. However, these large-scale bridging models often require iterative methods/algorithms that may sometimes have convergence problems associated with them.

A simpler large-scale bridging model was, therefore, employed in the current study. This model, which was first proposed by Bloyer et al. [11,12] and used in subsequent studies by Li and Soboyejo [13] and Lou and Soboyejo [14]. It utilizes weight functions by Fett and Munz [15], in the estimation of the weighted distributions of bridging traction across the individual reinforcements (Fig. 2). The shielding due to large-scale bridging, ΔK_{lsb}, may thus be expressed as:

$$\Delta K_{lsb} = \int_L \alpha\sigma(x)h(a,x)\,dx \quad (2)$$

where L is the length of the bridge zone, α is a constraint/triaxiality factor, $\sigma(x)$ is a traction function along the bridge zone, and $h(a,x)$ is a weight function given by Fett and Munz [15]:

$$h(a,x) = \sqrt{\frac{2}{\pi a}} \frac{1}{\sqrt{1-\frac{x}{a}}} \left[1 + \sum_{(v,\mu)} \frac{A_{v\mu}\left(\frac{a}{W}\right)}{\left(1-\frac{a}{W}\right)} \left(1-\frac{x}{a}\right)^{v+1}\right] \quad (3)$$

where a is the crack length and W is the specimen width. The resistance-curve behavior may now be estimated by a simple application of the principle of linear superposition. This gives the following expression for the estimation of the stress intensity factors along the resistance-curve:

$$K = K_i + \Delta K_{lsb} \quad (4)$$

where K_i is the initiation toughness required for renucleation ahead of the first ductile layer encountered by the propagating crack, and ΔK_{lsb} is given by Eq. (2) for large-scale bridging.

3. Experimental procedures

3.1. Material

The concrete material that was used in this study was produced at The Ohio State University, Columbus, OH. Concrete mixes with nominal compressive strength levels of 30, 35 and 40 MPa were obtained by the mixing of aggregates and cement in the ratios shown in Table 1. After mixing, the concrete was allowed to harden for the resistance-curve experiments at Princeton University, Princeton, NJ.

The resistance-curve experiments were conducted on single edge notched bend (SENB) specimens that were produced by introducing notches with a diamond wheel. The resulting specimen geometry is presented in Fig. 1. Resistance-curve experiments were conducted in a servo-hydraulic testing machine that was operated under load control. Crack growth during the resistance-curve experiments was monitored using a notch-mouth clip gauge and a Questar telescope (resolution of ~2.5 μm) that was connected to a video monitoring unit. In this way, the crack/microstructure interactions associated with crack nucleation and stable crack growth were studied, along with the crack-tip shielding mechanisms that can give rise to stable crack growth under monotonic loading.

Low initial loads corresponding to a stress intensity factor of ~0.2 MPa $m^{1/2}$ were applied initially. These were increased in steps of ~5–10% until crack growth was detected. After each incremental crack growth step, the loads were increased in steps of ~5% until stable crack growth occurred. In this way, resistance-curves were obtained for crack growth over several millimeters of stable crack growth. This was continued until final fracture occurred. The fracture surfaces of the specimens were then examined under a light microscope to reveal the underlying three-dimensional crack paths.

Table 1
Nominal composition of the three types of concrete

	Mix 30 MPa	Mix 35 MPa	Mix 40 MPa
Cement	Type I	Type I	Type I
	(1 part)	(1 part)	(1 part)
	456.59 kg/m^3	513.39 kg/m^3	609.26 kg/m^3
Coarse aggregate	Irregular gravel	Irregular gravel	Irregular gravel
	(2.672 parts)	(2.255 parts)	(1.808 parts)
	1220.23 kg/m^3	1172.42 kg/m^3	1101.57 kg/m^3
Fine aggregate	Well graded sand	Well graded sand	Well graded sand
	(0.890 parts)	(0.751 parts)	(0.602 parts)
	406.74 kg/m^3	390.47 kg/m^3	36.19 kg/m^3
Water/cement ratio	0.416	0.378	0.338
	190.18 l/m^3	196.84 l/m^3	206.37 l/m^3

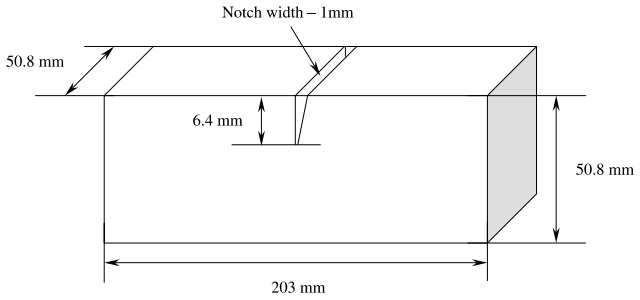

Fig. 1. Dimensions of SENB specimen.

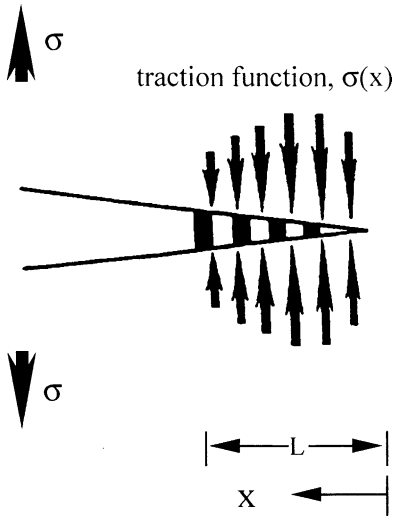

Fig. 2. Schematic representation of a large-scale bridging model (taken from [11]).

4. Results and discussion

4.1. Crack/microstructure interactions

Typical crack/microstructure interactions observed in the resistance-curve experiments are shown in Fig. 3a–c. These show the growth of dominant cracks, with uncracked bridging ligaments behind the crack-tip. Unlike most prior studies of stable crack growth in concrete [1–4,16], no zone of microcracks was observed ahead of the dominant cracks, as shown schematically in Fig. 4. Hence, the possible shielding/anti-shielding effects of microcracking [16] were neglected in subsequent analyses.

The crack/microstructure observations, therefore, revealed that stable crack growth occurred primarily as a result of crack bridging phenomena by uncracked ligaments that were left behind the crack-tip (Fig. 3a–c). The shielding effects due to such uncracked ligaments will be analyzed later using concepts described earlier in the section on micromechanical modeling.

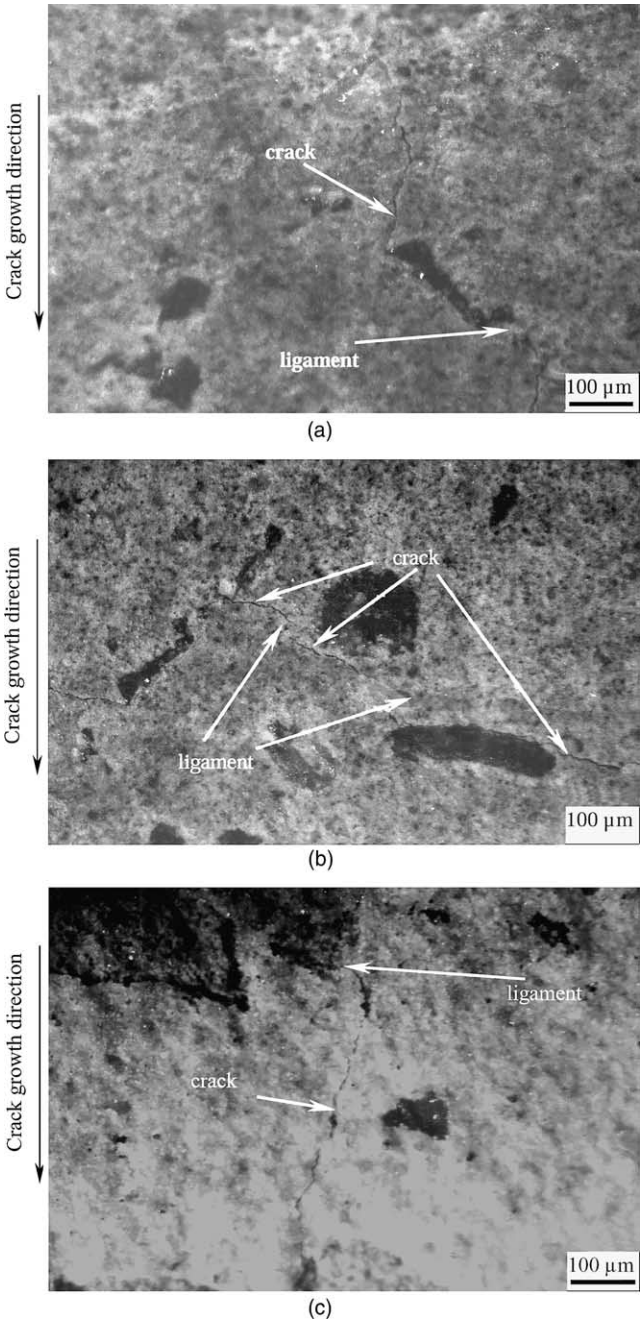

Fig. 3. Typical crack/microstructure interactions in concrete with strength levels of: (a) 30 MPa; (b) 35 MPa and (c) 40 MPa.

4.2. Resistance-curve behavior

The measured resistance-curves obtained for the three concrete specimens are presented in Fig. 5. This shows that initiation toughness and resistance-curve behavior improve with increase mixture strength between 30 and 40 MPa. The resistance-curve behavior of the 40 MPa concrete is considerable better than that of the 30 and 35 MPa concrete. However, the amount of stable crack growth increases with decreasing concrete strength (Fig. 5).

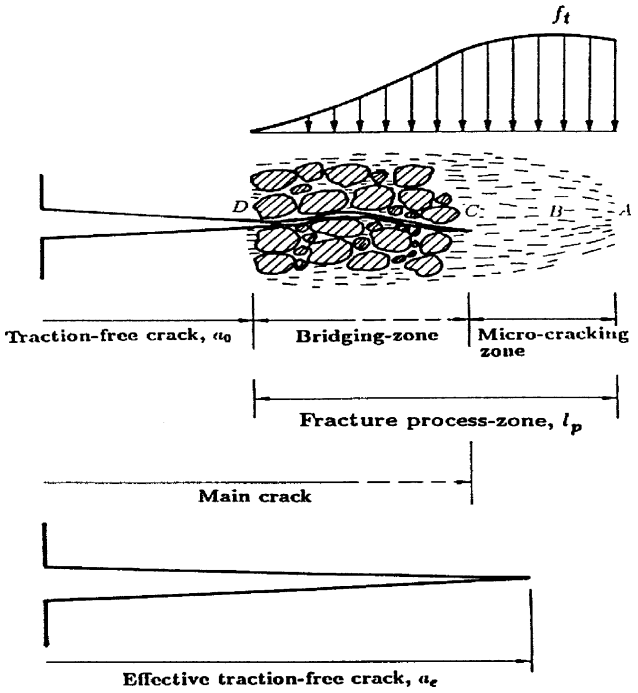

Fig. 4. Schematic illustration of microcracking and ligament bridging in concrete (taken from [21]).

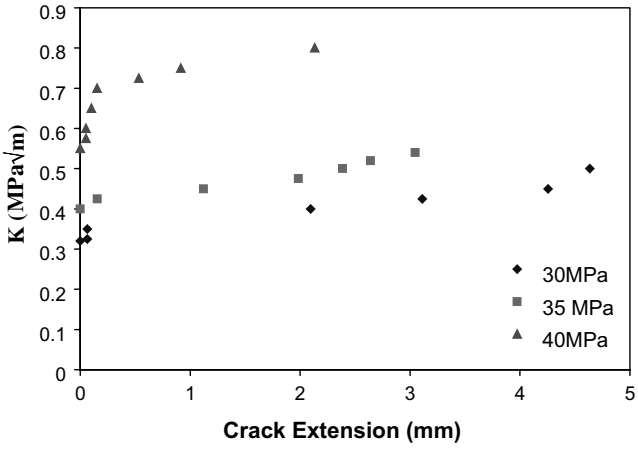

Fig. 5. Resistance-curve behavior of concrete for three different strengths.

4.3. Analysis of ligament bridging

Since the crack/microstructure interactions revealed the occurrence of ligament bridging, it is of interest to explore the extent to which the measured resistance-curves can be predicted by small- and large-scale ligament bridging models presented earlier in the section on micromechanical modeling. The bridge lengths that were used in the modeling were obtained from images of crack/microstructure interactions. They correspond to the distance from the crack-tip to the last unfractured ligament on a side profile.

Table 2
Constants in the large-scale bridging equation

v	μ				
	0	1	2	3	4
0	0.4980	2.4463	0.0700	1.3187	−3.067
1	0.5416	−5.0806	24.3447	−32.7208	18.1214
2	−0.19277	2.55863	−12.6415	19.7630	−10.986

Table 3
Summary of basic mechanical properties and parameters used in the small- and large-scale bridging model

Mechanical property and parameters	30 MPa concrete	35 MPa concrete	40MPa concrete
Youngs modulus (MPa)	31220	33721	36049
Compressive strength (MPa)	30	35	40
Volume fraction of ligament, V_l	0.1	0.1	0.1

Using material properties summarized in Tables 2 and 3 and Eqs. (1)–(4) from the micromechanical modeling section, the resistance-curves were predicted for stable crack growth in the small-scale bridging ($\Delta a < 0.5$ mm) and large-scale bridging ($\Delta a \geqslant 0.5$ mm) regimes. The results of the predictions are presented in Fig. 6a–c for concrete with different strength levels. These show the predicted resistance-curves obtained from Eqs. (1)–(4) for typical ligament volume fractions of ~0.1. In all cases, the predicted resistance-curves were comparable to the measured resistance-curves in the small- and large-scale bridging regimes. The small-scale bridging model captures the rapid rise in initial resistance-curve behavior ($\Delta a < 0.5$ mm), while the large-scale bridging model captures the trends in subsequent resistance-curve behavior ($\Delta a \geqslant 0.5$ mm) (Fig. 6a–c).

It is important to note that the above agreement was achieved without the use of any fitting functions. The modeling approach presented in this paper, therefore, appears to provide a robust framework for the estimation of resistance-curve behavior. The approach has the advantage of being simple to implement. It may, therefore, be applied readily to the design of durable concrete mixes.

However, more complex bridging models may be applied in cases where very high accuracy is needed in the quantification of crack bridging [3–6,17–22]. Such models require the use of stress–displacement functions that are difficult to obtain. They are also highly prone to numerical instabilities during iterative implementation steps.

4.4. Crack deflection analysis

It is also important to note here that the analysis of the fracture surfaces revealed some crack deflection

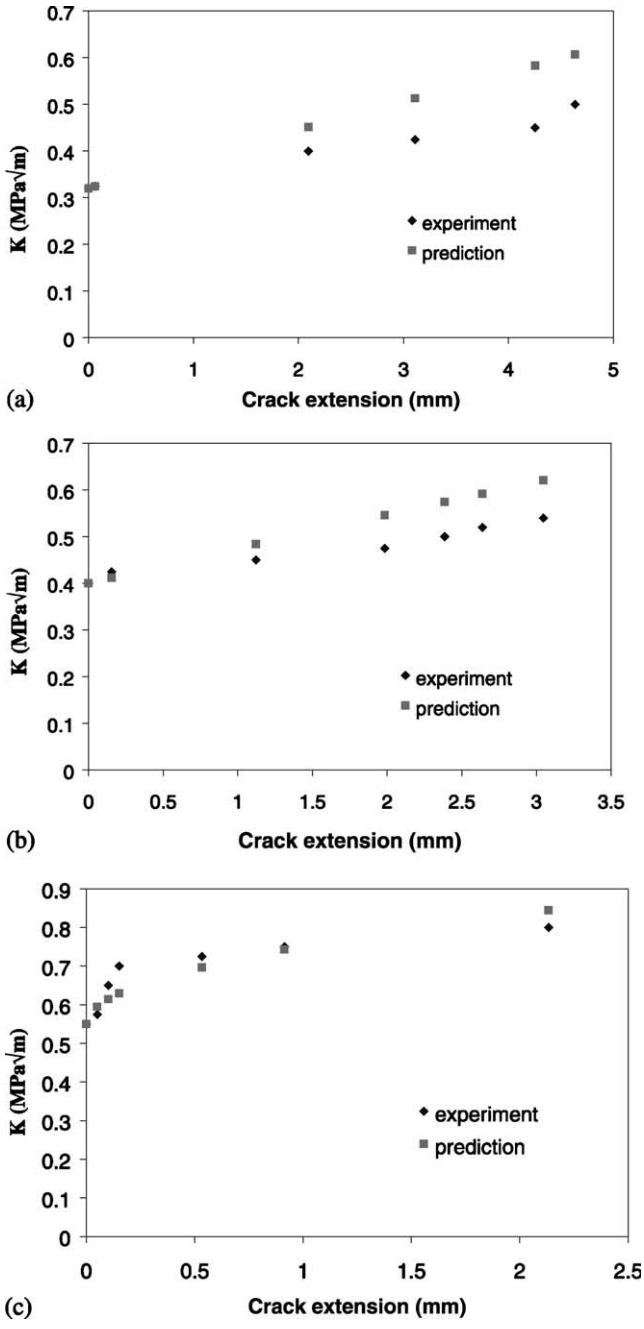

Fig. 6. Comparison of the experimental and predicted resistance-curve behavior for concrete with the strength levels of: (a) 30 MPa; (b) 35 MPa and (c) 40 MPa.

around the aggregates. This is shown clearly in Fig. 7a–c for the three mixes that were examined in the current study. The shielding components form such three-dimensional crack deflection mechanisms are difficult to assess rigorously. However, shielding estimates may be obtained from the following expression derived originally for cracks with deflected segments that are comparable to the undeflected segments. For such cracks, toughening ratio due to deflection by tilting through an angle, θ, is given by [23,24]:

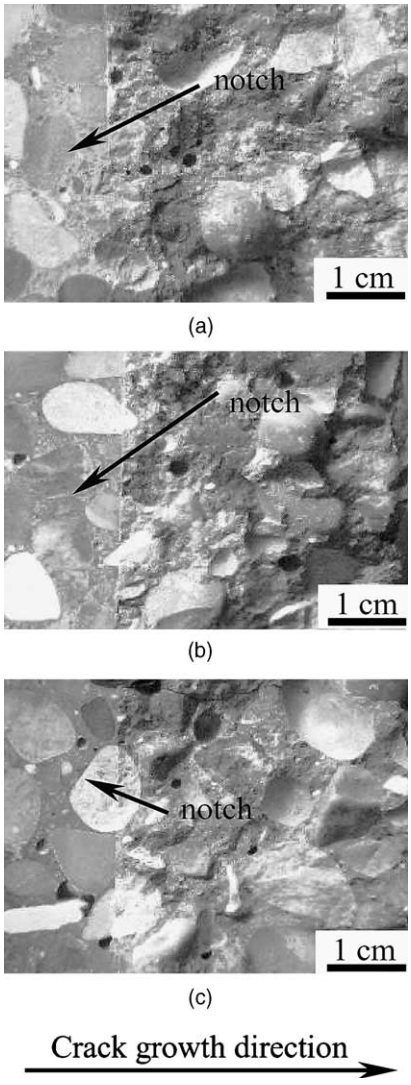

Fig. 7. Typical fracture modes in concrete with strength levels of (a) 30 MPa; (b) 35 MPa and (c) 40 MPa.

$$\lambda_d = \frac{K}{K_m} = \frac{1}{\cos^2\theta} \tag{5}$$

where K_m is the matrix toughness and K is the remote toughness. The overall toughening, ΔK_d, due to crack deflection is, therefore, given by:

$$\Delta K_d = (\lambda_d - 1)K_m \tag{6}$$

For the most extreme cases in the current study, $\theta \sim 45°$. In such cases, $\lambda_d \sim 1.17$, and $\Delta K_d \sim 0.05$ MPa m$^{1/2}$ from Eq. (6). Hence, the shielding contributions from crack deflection are quite small, and can be neglected.

4.5. Intrinsic toughness

The resistance-curve presented in Figs. 5 and 6 are all specimen dependent. Hence, they do not represent true material properties. In an effort to obtain true material properties, Bloyer et al. [11,12] suggested that the weight

Table 4
Steady-state toughness values for concrete

Concrete strength	Steady-state toughness values (MPa $m^{1/2}$)
30 MPa	0.712
35 MPa	0.724
40 MPa	0.822

function in Eq. (3) may be used to estimate the bridging tractions for infinitely wide specimens. The asymptotic values of ΔK_b obtained as W is extrapolated towards infinity correspond to the intrinsic small-scale steady-state toughness of the concrete mixes. They are true material properties that are independent of specimen dimensions.

The extrapolated steady-state toughness values obtained from the current work are shown in Table 4. These show that the intrinsic steady-state toughness increases from ~0.71 MPa $m^{1/2}$ for the 30 MPa concrete, to 0.72 MPa $m^{1/2}$ for the 35 MPa concrete and 0.82 MPa $m^{1/2}$ for the 40 MPa concrete. Hence, the intrinsic steady-state toughness increases with increasing concrete strength. This is an important result that would be difficult to obtain within an experimental framework in which very large specimens would have to be tested to obtain the small-scale bridging steady-state toughness values.

5. Implications

The implications of the current work are very significant. First, the measured resistance-curves suggest that the fracture initiation toughness and resistance-curve behavior (of the selected concrete mixes with strength levels between 30 and 40 MPa) improve with concrete strength. Hence, mix design for improved strength may be accomplished without compromising fracture toughness.

However, there is an inverse relationship between mix strength and fatigue crack growth resistance [25]. Hence, the mixes that exhibit the greatest fatigue resistance also have lower strength and fracture initiation toughness/resistance-curve behavior. Viceversa, systems with lower fatigue crack growth resistance exhibit improved fracture initiation toughness/resistance-curve behavior. This is shown in Figs. 5 and 8 in which the respective resistance-curves and fatigue crack growth curves are presented for concrete with strength levels of 30, 35 and 40 MPa $m^{1/2}$ (Fig. 8).

The design of durable concrete mixtures, therefore, requires a balanced consideration of strength, fracture initiation toughness/resistance-curve behavior and fatigue crack growth resistance. This is clearly the challenge for future mix designers that must select durable concrete mixes with the desired balance of properties.

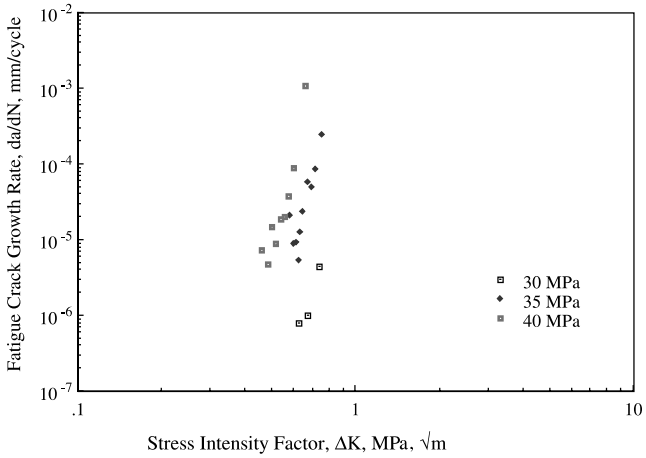

Fig. 8. Fatigue crack growth rate data obtained from concrete with strength levels of 30, 35 and 40 MPa.

6. Conclusions

The fracture initiation toughness and resistance-curve behavior of concrete mixes with strength levels of 30, 35 and 40 MPa has been studied. The following conclusions have been reached from a combined experimental and theoretical study:

1. The fracture initiation toughness increases with increasing mixture strength. The mix with a strength of 30 MPa has the lowest fracture initiation toughness of ~0.3 MPa $m^{1/2}$, while the 40 MPa mix has the highest initiation fracture toughness of ~0.6 MPa $m^{1/2}$. The 35 MPa mix has an intermediate fracture toughness of ~0.4 MPa $m^{1/2}$.
2. The trends in the measured resistance-curves are similar to those in the fracture initiation toughness. The resistance-curve behavior, therefore, improves with the increasing mixture strength. Hence, mix design for strength and toughness can be achieved readily.
3. The intrinsic steady-state fracture toughness increases with increasing mix strength. The 30 MPa concrete has an intrinsic fracture toughness of ~0.71 MPa $m^{1/2}$ m, while the 35 MPa concrete has an intrinsic fracture toughness of ~0.72 MPa $m^{1/2}$. The 40 MPa concrete has the highest intrinsic fracture toughness of ~0.82 MPa $m^{1/2}$. The intrinsic fracture toughness values provide a measure of crack growth resistance that is independent of specimen dimensions. They are ''true'' material properties.
4. However, the fatigue crack growth resistance of the selected concrete mixes decreases with increasing mixture strength/fracture toughness. This suggests that a balanced approach is needed in the design of concrete mixtures with the required combination of strength, fracture toughness and fatigue crack growth resistance.

Acknowledgements

The research is supported by The Division of Mechanics and Materials of The National Science Foundation, with Dr. Ken Chong as Program Monitor. Appreciation is also extended to Dr. Dan Davis for his encouragement and support of this work.

References

[1] Karihaloo BL, Nallathambi P. Cement Concrete Res 1989;19:603.
[2] Jeng Y-S, Shah SP. J Eng Mech 1985;111:1227.
[3] Bazant ZP, Kim JK, Pfeiffer PA. J Struct Eng 1986;112:289.
[4] RILEM FMC-50, RILEM, Materiux et Constructions, 18:287.
[5] Budiansky B, Amazigo JC, Evans AG. J Mech Phys Solids 1988;36:167.
[6] Tada H, Paris PC, Irwin GR. The stress analysis of cracks handbook. New York, NY: ASME; 1999.
[7] Odette GR, Chao BL, Sheckherd JW, Lucas GE. Acta Metall Mater 1992;40:2381.
[8] Zok F, Hom CL. Acta Metall Mater 1990;38:1895.
[9] Cox BN, Lo CS. Acta Metall Mater 1992;40:69.
[10] Cox BN, Rose LRF. Mech Mater 1996;22:249.
[11] Bloyer DR, Venkateswara Rao KT, Ritchie RO. Metall Mater Trans A 1998;29A:2483.
[12] Bloyer DR, Venkateswara Rao KT, Ritchie RO. Metall Mater Trans A 1999;30A:633.
[13] Li M, Soboyejo WO. Metall Mater Trans A 2000;31A:1385.
[14] Lou J, Soboyejo WO. Metall Mater Trans A 2001;32A:325.
[15] Fett T, Munz D. Stress intensity factors and weight functions for one-dimensional cracks. Kernforschungszentrum, Karlsryhe, Germany: Institut fur Materialforschung; 1994.
[16] Karihaloo BL, Nallathambi P. In: Shah SP, editor. Toughening Mechanics Quasi-Brittle Materials. Dordrecht, The Netherlands: Kluwer Academic Publishers; 1990.
[17] Cox BN, Marshall DB. Acta Metall Mater 1991;39:579.
[18] Cox BN, Francis Rose LR. Mech Mater 1996;22:249.
[19] Odette GR, Chao BL, Sheckherd JW, Lucas GE. Acta Metall Mater 1992;40:2381.
[20] Zok F, Hom CL. Acta Metall Mater 1990;38:1895.
[21] Li VC, Chan CM, Leung KY. Cement Concrete Res 1987;17:441.
[22] Bao G, Suo Z. Appl Mech Rev 1992;45:355.
[23] Suresh S, Brockenbrough JR. Acta Metall 1988;36:1444.
[24] Bilby BA, Cardew GE, Howard IC. Fracture B 1977:197.
[25] Bhalerao K, Shen W, Soboyejo ABO, Soboyejo WO. A multiparameter framework for the modeling of fatigue crack growth in concrete. Cement Concrete Compos, submitted for publication.